Modified predictive formula for the electron stopping power

A. Jablonski,[1] S. Tanuma,[2] and C. J. Powell[3,a)]
[1]Institute of Physical Chemistry, Polish Academy of Sciences, ul. Kasprzaka 44/52, 01-224 Warsaw, Poland
[2]Materials Analysis Station, National Institute for Materials Science, 1-2-1 Sengen, Tsukuba, Ibaraki 305-0047, Japan
[3]Surface and Microanalysis Science Division, National Institute of Standards and Technology, Gaithersburg, Maryland 20899-8370, USA

(Received 1 November 2007; accepted 3 January 2008; published online 19 March 2008)

We report an improved predictive formula for the electron stopping power (SP) based on an analysis and fit of SPs and electron inelastic mean free paths (IMFPs) calculated from optical data for 37 elemental solids and energies between 200 eV and 30 keV. The formula is a function of energy, density, and IMFP, and is recommended for solids with atomic numbers larger than 6. While the mean deviation between predicted and calculated SPs was 7.25%, larger deviations were found for four additional materials, Li (22.2%), Be (17.9%), graphite (15.3%), and diamond (15.7%). The predictive SP formula can be applied to multicomponent materials. Test comparisons for two compounds, guanine and InSb, showed average deviations of 16.0% and 19.1%, respectively. The improved SP formula is expected to be useful in simulations of electron trajectories in solids with the continuous slowing-down approximation (e.g., in Auger-electron spectroscopy and electron microprobe analysis). © *2008 American Institute of Physics*. [DOI: 10.1063/1.2891047]

I. INTRODUCTION

Quantification of Auger-electron spectroscopy (AES) and electron microprobe analysis (EPMA) should be based on a reliable theoretical model describing the transport of the primary-electron beam impinging on the sample surface. Monte Carlo (MC) simulations are often used to obtain a relation between the signal intensity and the concentration of a given element in the surface region. In principle, we need to determine primary-electron trajectories in the solid by simulating individual elastic- and inelastic-scattering events. This approach, however, is generally difficult due to the lack of sufficient data describing the differential inelastic-scattering cross section as a function of energy loss; in addition, it may not be easy to construct accurate statistical samplers for materials with complex structure in this differential cross section.[1] In computational practice, these difficulties are circumvented by using the continuous slowing-down approximation (CSDA) in which it is assumed that the electron energy along a trajectory is a function of the trajectory length. A crucial parameter needed in the relevant MC algorithm is the stopping power (SP) which is defined as the energy change, dE, per increment of distance, dx, along the trajectory, $S=-dE/dx$. The CSDA and SP data are also used in modeling electron transport in solids for other applications.

The concept of SP has a long history in theories of electron transport. Over seven decades ago, Bethe[2] developed a now well-known formula in which the SP is expressed, for nonrelativistic energies, as

$$S=-\frac{dE}{dx}=2\pi e_0^4 N_0 \frac{Z\rho}{AE}\ln\left(\frac{\sqrt{(e/2)}E}{J}\right)$$
$$=785\frac{Z\rho}{AE}\ln\left(\frac{1.166E}{J}\right) \quad (\text{in eV/Å}), \tag{1}$$

where e_0 is the electron charge, e is the base for natural logarithms, N_0 is the Avogadro constant, Z is the atomic number, ρ is the density (in g/cm^3), A is the atomic mass, E is the electron energy (in eV), and J is the mean excitation energy (in eV). The constant $\sqrt{(e/2)}\approx 1.166$ takes into account electron-exchange effects. Extensive compilations of calculated and measured SPs for numerous elements and compounds are available.[3–5]

The Bethe formula is expected to be valid for relatively high primary-electron energies, i.e., energies exceeding the K-shell binding energies of all atoms constituting the sample.[6] The reliability of the Bethe equation seems to be sufficient, however, in calculations of parameters needed in EPMA, and this equation is recommended for use for primary-beam energies between 15 and 30 keV.[7] Nevertheless, analyses of calculated SPs for Al (where the K-shell binding energy is 1.56 keV) indicate that the Bethe equation is valid only for energies larger than about 10 keV, and larger minimum energies for validity of the Bethe equation are likely for higher atomic numbers.[8]

It should also be noted that SPs from Eq. (1) become negative when $E<J/1.166$, an obviously unrealistic result. Several attempts have been made to modify the Bethe equation so that it can be used at low energies. Rao-Sahib and Wittry[9] proposed a parabolic extrapolation of the Bethe equation for $E<6.388J$; this extrapolation does not have any physical basis, and was introduced only for computational convenience. For example, their approach was used by Love *et al.*[10] in calculations of so-called "Phi-Rho-Z" curves for

a)Electronic mail: cedric.powell@nist.gov.

quantitative EPMA. Other modifications to the Bethe equation have been proposed by Joy and Luo[11] and by Fernandez-Varea *et al.*[12] Although the proposed extensions described SPs at low energies quite well, the relevant formulas are applicable to only a limited number of solids for which the needed parameters are available.

In AES, we need to follow the electron energies down to the ionization energies of core shells, generally below 1 keV. It is then critical, for MC simulations using the CSDA, to have reliable SPs at these energies. Attempts have been made to use the Bethe equation in calculations of the backscattering factor for AES, and a sophisticated algorithm has been proposed to avoid computational problems at low energies.[13–15] A similar approach has been used in calculations of the energy dependence of the Auger-electron current and of the angular and energy distributions of electrons backscattered from solids.[16] Due to the complexity of this algorithm, however, it has not been utilized by others.

In principle, one can derive a SP for any solid from Tougaard's universal inelastic-scattering cross-section formulas.[17] The SP can be expressed in terms of the mean energy loss, $\Delta T(E)$, in an inelastic-scattering event and the inelastic mean free path (IMFP), λ_{in}:[1]

$$S = -\frac{dE}{dx} \approx -\frac{\Delta E}{\Delta x} = \frac{\Delta T(E)}{\lambda_{in}}. \tag{2}$$

Although expressions can be derived for $\Delta T(E)$,[1] the Tougaard formulas were developed for energy losses less than 50 eV; i.e., they did not include the contributions due to core-electron excitations that are significant for the SP.[8] In addition, the Tougaard formulas were obtained for electron energies between 300 and 1500 eV, and may not be useful for energies outside this range. We therefore do not think it useful to compute S from Eq. (2) with $\Delta T(E)$ from the Tougaard formulas.

An attempt has been made recently to derive a universal SP expression by approximation of the energy dependence of the $S\lambda_{in}$ product (the so-called S-lambda approach).[18,19] The recommended expression, obtained from an analysis of SPs and IMFPs calculated from optical data for a group of 27 elemental solids for energies between 200 eV and 30 keV, has the form

$$S\lambda_{in} = \Delta T(E) = c_1(c_2 Z + 1)\ln(c_3 E) \text{ (in eV)}, \tag{3}$$

where Z is the atomic number, E is expressed in eV, λ_{in} is expressed in Å, and $c_1 = 11.52$, $c_2 = 0.016\,39$, and $c_3 = 0.033\,86$ are coefficients derived from a fit to the product of the calculated SPs and IMFPs. The mean percentage deviation between SPs calculated from Eq. (3) and from optical data, averaged over the 27 elements, was found to be 10.4%.[18]

The product $S\lambda_{in}$ is generally a monotonically increasing function of energy, with a relatively smooth shape.[18] Thus, the derivation of an expression fitted to a large database of SP and IMFP data seems to be a promising approach for a predictive formula providing SPs over a large energy range. In the present work, we present an improved SP predictive formula based on the S-lambda approach. First, we consider SPs and IMFPs calculated from optical data for 14 additional elemental solids. Second, we consider an improved approximating expression for S-lambda. We present a brief description of the SP and IMFP calculations in the following section and explain the basis of our S-lambda expression. We then present comparisons of SPs from the improved expression with the calculated SPs in Sec. III. These results are discussed in Sec. IV.

II. THEORY

A. Calculations of IMFPs and SPs from optical data

A total inelastic-scattering cross section (or, equivalently, an IMFP) can be found from a model dielectric function $\varepsilon(q,\omega)$, a function of momentum transfer q, and energy loss $T = \hbar\omega$.[20] The differential inelastic-scattering cross section, per atom or molecule, in an infinite medium is

$$\frac{d^2\sigma}{dq d\omega} = \frac{m_0 e_0^2}{\pi N \hbar E} \operatorname{Im}\left(\frac{-1}{\varepsilon(q,\omega)}\right)\frac{1}{q}, \tag{4}$$

where m_0 is the electronic rest mass, N is the density of atoms or molecules per unit volume, and $\operatorname{Im}[-1/\varepsilon(q,\omega)]$ is the energy-loss function (ELF). The dependence of the ELF on ω can be obtained from experimental optical data for the material of interest (for $q=0$) while the dependence of the ELF on q can be obtained from an appropriate theoretical model.[20]

The IMFP and SP were determined using Penn's single-pole approximation[21] from the following integrals of $\operatorname{Im}[-1/\varepsilon(q,\omega)]/q$ and $\operatorname{Im}[-1/\varepsilon(q,\omega)](\omega/q)$, respectively, over the kinematically allowed regions of q and ω:

$$\lambda_{in}^{-1} = \frac{1}{\pi a_0 E}\int_0^\infty \omega_p \operatorname{Im}\left(\frac{-1}{\varepsilon(\omega_p)}\right)d\omega_p \int_{q^-}^{q^+}\frac{dq}{q\omega_p(q)} \times \int_0^{E-E_f} d(\hbar\omega)\,\delta[\omega - \omega_p(q)] \tag{5}$$

and

$$S = \frac{1}{\pi a_0 E}\int_0^\infty \omega_p \operatorname{Im}\left(\frac{-1}{\varepsilon(\omega_p)}\right)d\omega_p \int_{q^-}^{q^+}\frac{dq}{q\omega_p(q)} \times \int_0^{E-E_f} (\hbar\omega)\,d(\hbar\omega)\,\delta[\omega - \omega_p(q)], \tag{6}$$

where

$$\omega^2{}_p(q) = \omega^2{}_p + \tfrac{1}{3}[v(\omega_p)q]^2 + (\hbar q^2/2m_0)^2,$$

$$q^{\pm} = (\sqrt{2m_0 E}/\hbar)[1 \pm \sqrt{1 - (\hbar\omega/E)}],$$

$v(\omega_p)$ is the Fermi velocity of a free-electron gas with plasma frequency ω_p, and a_0 is the Bohr radius.

B. Improved predictive formula for the stopping power

The mean electron energy loss per inelastic interaction, $\Delta T(E)$, can be defined as

$$\Delta T(E) = \frac{\int_0^E TK(E,T)dT}{\int_0^E K(E,T)dT}, \tag{7}$$

where T is the actual energy loss per inelastic interaction, and $K(E,T)$ is the differential inelastic-scattering cross section.

We assume, as in our previous work,[18] that $\Delta T(E)$ is a product of several functions, with each of these functions providing a dependence on only one parameter, i.e., electron energy, density of the solid, and atomic number. That is,

$$\Delta T(E) = F(E)G(\rho)H(Z). \tag{8}$$

Appropriate functional forms of F, G, and H can be determined by minimization of the mean percentage deviation, $\langle \Delta S \rangle$, defined by

$$\langle \Delta S \rangle = 100 \frac{1}{N_Z N_E} \sum_{i=1}^{N_Z} \sum_{j=1}^{N_E} \frac{|S_{i,j} - S_{\text{fit}}(E_j, \rho_i, Z_i)|}{S_{i,j}}, \tag{9}$$

where N_Z is the number of elements, N_E is the number of energies, and

$$S_{\text{fit}}(E,\rho,Z) = \frac{F(E)G(\rho)H(Z)}{\lambda_{\text{in}}}. \tag{10}$$

For this analysis, we need an extensive set of SPs and IMFPs for a range of elemental solids and energies as well as suitable functions $F(E)$, $G(\rho)$, and $H(Z)$. The procedure used to obtain these functions is outlined in the following section.

III. RESULTS

In our derivation of the S-lambda expression in Eq. (3),[18] we considered IMFPs and SPs calculated from optical data for 27 solid elements (C-glassy, Mg, Al, Si, Ti, V, Cr, Fe, Ni, Cu, Y, Zr, Nb, Mo, Ru, Rh, Pd, Ag, Hf, Ta, W, Re, Os, Ir, Pt, Au, and Bi) and electron energies between 200 eV and 30 keV. In the present work, we also consider similarly calculated IMFPs and SPs for 14 additional solid elements (Li, Be, C-graphite, C-diamond, Na, K, Sc, Ge, In, Sn, Cs, Gd, Tb, and Dy). The IMFPs (Ref. 22) and SPs (Refs. 8 and 23) were calculated for energies evenly distributed on a logarithmic scale with energy increments of 10%. ELFs for these solids were checked for internal consistency using the f-sum rule and the perfect-screening sum rule.[24–26] These sum rules were satisfied with an average root-mean-square error of about 8.5%.

To fit Eq. (10) to the calculated SPs and IMFPs for the 41 elemental solids, we need suitable functional forms for the functions $F(E)$, $G(\rho)$, and $H(Z)$. At first, we considered the energy dependence of the SP for a given element. On testing different expressions, the following functional form of $F(E)$ was found to provide a satisfactory approximation to the calculated SPs:

$$F(E) = DE^{d_2^*} \ln(d_3^* E), \tag{11}$$

where $D = G(\rho)H(Z)$ for a given element, d_2^* and d_3^* are parameter values for a particular solid, and E is again expressed in eV. Approximations of SPs calculated for the ith element were then made from fits with the resulting expression:

TABLE I. Coefficients D, d_2^*, and d_3^* in Eq. (11) and the mean percentage deviations, ΔS_i, obtained from fits of Eq. (13) to the calculated SPs and IMFPs for each solid.

Z	D	d_2^*	d_3^* (eV^{-1})	ΔS_i (%)
3	18.246	−0.131 42	$3.413\,1 \times 10^{-2}$	0.71
4	29.624	−0.130 88	$3.392\,1 \times 10^{-2}$	0.43
6(gr)[a]	16.551	$-7.339\,1 \times 10^{-2}$	0.159 19	1.18
6(di)[a]	21.518	$-7.487\,4 \times 10^{-2}$	0.143 62	1.35
6(gc)[a]	18.511	$-6.885\,5 \times 10^{-2}$	$6.813\,8 \times 10^{-2}$	2.02
11	25.715	−0.105 46	$1.974\,2 \times 10^{-2}$	1.11
12	34.915	−0.114 19	$1.993\,5 \times 10^{-2}$	0.76
13	37.186	−0.108 80	$1.685\,8 \times 10^{-2}$	0.84
14	40.822	−0.114 38	$1.476\,6 \times 10^{-2}$	1.02
19	7.9016	$3.399\,0 \times 10^{-4}$	$6.282\,3 \times 10^{-2}$	3.11
21	9.0611	$-3.477\,7 \times 10^{-3}$	0.437 56	1.80
22	8.5371	$2.696\,2 \times 10^{-2}$	0.398 66	1.90
23	7.8451	$5.076\,2 \times 10^{-2}$	0.164 10	2.39
24	12.812	$8.100\,6 \times 10^{-3}$	0.128 88	1.56
26	16.286	$-4.240\,2 \times 10^{-4}$	$8.220\,2 \times 10^{-2}$	1.40
28	34.064	$-5.203\,7 \times 10^{-2}$	$3.512\,6 \times 10^{-2}$	0.98
29	40.656	$-5.702\,2 \times 10^{-2}$	$2.266\,7 \times 10^{-2}$	0.91
32	34.274	$-5.747\,7 \times 10^{-2}$	$1.535\,8 \times 10^{-2}$	0.92
39	17.873	$-1.490\,8 \times 10^{-2}$	$3.735\,7 \times 10^{-2}$	2.35
40	12.151	$2.512\,9 \times 10^{-2}$	$5.255\,9 \times 10^{-2}$	2.79
41	12.373	$4.654\,3 \times 10^{-2}$	$6.090\,7 \times 10^{-2}$	3.48
42	9.9804	$5.032\,6 \times 10^{-2}$	0.142 26	3.16
44	4.4029	0.108 22	2.057 6	3.70
45	5.3009	$9.465\,0 \times 10^{-2}$	1.555 7	3.49
46	5.3239	0.121 22	0.311 93	4.29
47	17.917	$7.683\,0 \times 10^{-4}$	0.130 39	2.73
49	6.3796	$7.522\,3 \times 10^{-2}$	0.607 86	2.43
50	8.2325	$6.267\,3 \times 10^{-2}$	0.372 64	2.34
55	6.1942	$5.320\,6 \times 10^{-2}$	$6.248\,3 \times 10^{-2}$	2.79
64	12.167	$3.368\,6 \times 10^{-2}$	$5.730\,1 \times 10^{-2}$	1.24
65	12.297	$2.103\,0 \times 10^{-2}$	$9.371\,2 \times 10^{-2}$	0.77
66	15.128	$1.294\,6 \times 10^{-2}$	$6.566\,2 \times 10^{-2}$	0.72
72	18.776	$4.378\,7 \times 10^{-2}$	$2.547\,3 \times 10^{-2}$	1.24
73	16.960	$3.693\,0 \times 10^{-2}$	$4.880\,0 \times 10^{-2}$	1.06
74	16.554	$4.142\,8 \times 10^{-2}$	$4.921\,3 \times 10^{-2}$	1.33
75	15.239	$3.760\,8 \times 10^{-2}$	0.101 21	1.19
76	16.594	$4.691\,6 \times 10^{-2}$	$5.535\,6 \times 10^{-2}$	1.48
77	14.588	$6.453\,5 \times 10^{-2}$	$4.973\,9 \times 10^{-2}$	1.86
78	13.547	$6.227\,2 \times 10^{-2}$	$6.936\,9 \times 10^{-2}$	2.01
79	10.341	$6.675\,8 \times 10^{-2}$	0.295 62	1.69
83	6.9828	$8.904\,2 \times 10^{-2}$	0.259 46	2.08

[a]For $Z=6$, (gr) corresponds to graphite, (di) to diamond, and (gc) to glassy carbon.

$$S_{\text{fit}}(E) = \frac{DE^{d_2^*} \ln(d_3^* E)}{\lambda_{\text{in}}}, \tag{12}$$

as follows from Eqs. (2), (8), and (11). The fit was performed by minimization with respect to D, d_2^*, and d_3^* of the following mean percentage deviation, $\langle \Delta S_i \rangle$:

$$\Delta S_i = 100 \frac{1}{N_E} \sum_{j=1}^{N_E} \frac{|S_{i,j} - S_{\text{fit}}(E_j)|}{S_{i,j}}. \tag{13}$$

The fit coefficients and the minimum percentage deviations are listed in Table I for each solid. We see from the relatively small values of $\langle \Delta S_i \rangle$ that the proposed function describes the

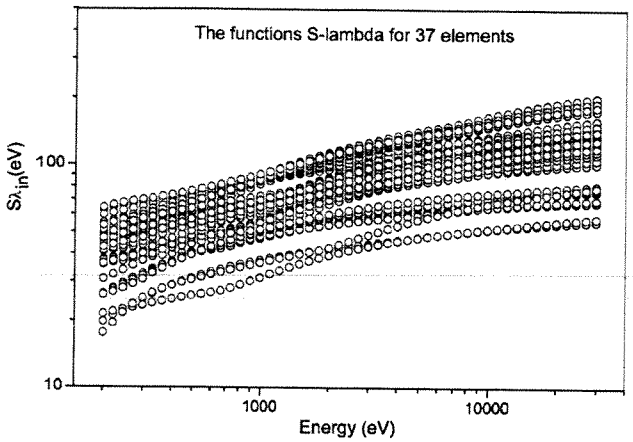

FIG. 1. Product of the SP and the IMFP, $S\lambda_{in}$, for 37 elemental solids as a function of electron energy.

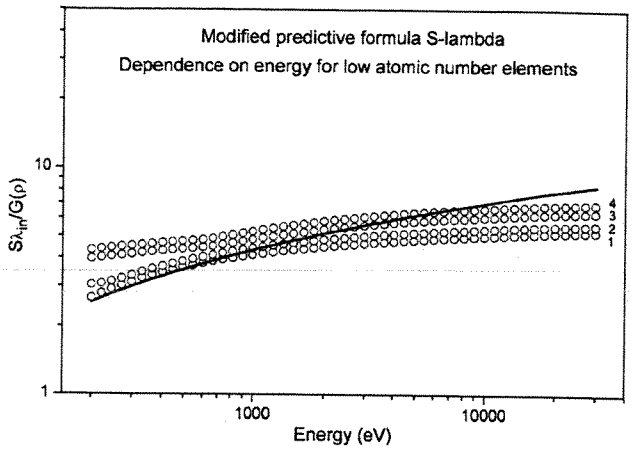

FIG. 3. Same as Fig. 2 except for the four low-Z solids: (1) Li, (2) Be, (3) graphite, and (4) diamond.

energy dependence of the SP very well. In the majority of cases, $\langle \Delta S_i \rangle$ is less than 2%; in the worst case (Pd), $\langle \Delta S_i \rangle$ is 4.29%. Although there is no known theoretical justification for the form of Eq. (11), this equation provides a convenient description of the SP energy dependence for the 41 elemental solids. On comparison with Eq. (3), we see that the energy dependence proposed here is slightly more complicated than for our previous SP expression.

In a similar way, we determined the functional dependences of the calculated SPs on density and atomic number, i.e., the functions $G(\rho)$ and $H(Z)$. In the second stage, we assumed that the dependence of the product $S\lambda_{in}$ on density could be described by

$$G(\rho) = d_1(\rho + d_4)^{d_5}, \tag{14}$$

where ρ is expressed in g/cm^3. The minimization was performed simultaneously for all elements and energies. The minimized function was again the mean percentage deviation:

$$\langle \Delta S \rangle = 100 \frac{1}{N_Z N_E} \sum_{i=1}^{N_Z} \sum_{j=1}^{N_E} \frac{|S_{i,j} - S_{\text{fit}}(E_j, \rho_i)|}{S_{i,j}}, \tag{15}$$

where

$$S_{\text{fit}}(E, \rho) = \frac{d_1 E^{d_2} \ln(d_3 E)(\rho + d_4)^{d_5}}{\lambda_{in}}. \tag{16}$$

It was found that Eq. (16) described well the calculated SPs for most elements, although larger deviations were found for the two elements with the smallest atomic number (Li and Be). In addition, large deviations were found in the fits for graphite and diamond. We eventually decided to omit these four low-Z materials in our fits. The minimization procedure, extended over 37 elements, resulted in the following values for the parameters d_i in Eq. (16):

$$d_1 = 7.892\,71,$$

$$d_2 = 0.011\,708\,8,$$

$$d_3 = 0.054\,512\,6,$$

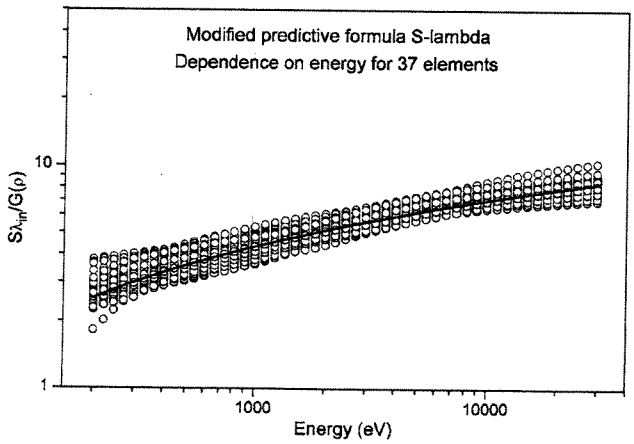

FIG. 2. Energy dependence of the function $S\lambda_{in}/G(\rho)$ for 37 elemental solids. This function is proportional to $F(E)$, and has been obtained by dividing the product $S\lambda_{in}$ (in units of eV) for each solid and energy by the expression $G(\rho)=d_1(\rho+d_4)^{d_5}$ [see Eq. (14)]. The solid lines in both panels show the function $F(E)=E^{d_2}\ln(d_3E)$ [see Eq. (17)].

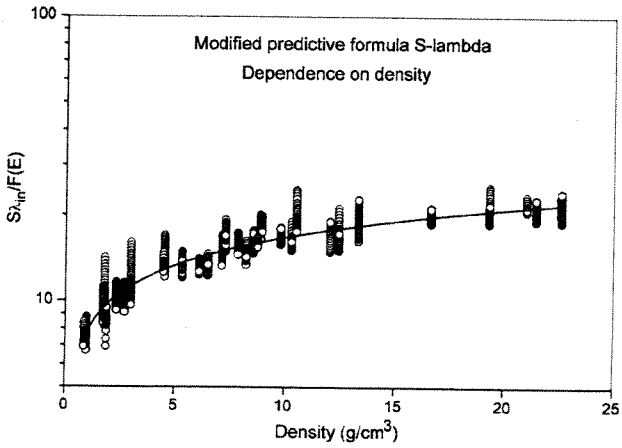

FIG. 4. Density dependence of the function $S\lambda_{in}/F(E)$. This function is proportional to the contribution $G(\rho)$, and has been obtained by dividing the product $S\lambda_{in}$ (in units of eV) by the expression $F(E)=E^{d_2}\ln(d_3E)$ [see Eq. (17)]. The solid line shows the function $G(\rho)=d_1(\rho+d_4)^{d_5}$ [see Eq. (14)].

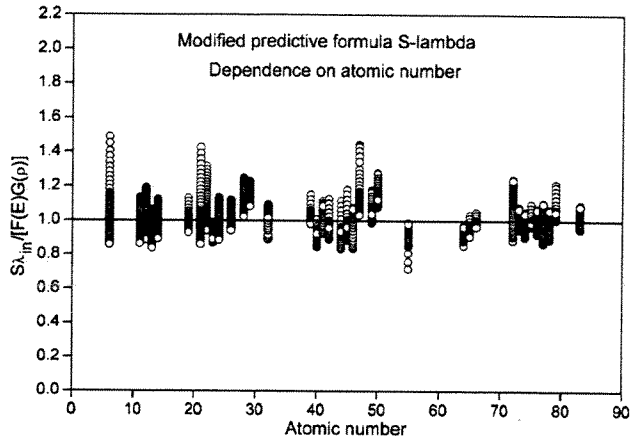

FIG. 5. Atomic number dependence of the function $S\lambda_{in}/[F(E)G(\rho)]$. This function has been obtained by dividing the product $S\lambda_{in}$ (in units of eV) by the expression $d_1E^{d_2}\ln(d_3E)(\rho+d_4)^{d_5}$ [see Eqs. (14) and (17)]. The solid line shows unity.

$$d_4 = -0.025\,448\,8,$$

$$d_5 = 0.326\,907.$$

The minimum value of $\langle \Delta S \rangle$ from Eq. (15) is now 7.25%, a value that is much lower than that found previously using Eq. (3) as the fitting function (10.44% obtained for a fit to SPs for only 27 elemental solids).[18]

Figure 1 shows products of the SPs and IMFPs, $S\lambda_{in}$, calculated from optical data for the 37 elements as a function of energy. As indicated in our previous work, the products are a monotonically increasing function of energy.[18] The plots have generally similar shapes for all elements but exhibit a considerable spread. To visualize the dependence on energy only, we plot the function $S\lambda_{in}/G(\rho)$ for 37 elements in Fig. 2. We see that the spread in this function is much less than the spread in Fig. 1 (and also much less than the spread in Fig. 1 of Ref. 18). The solid line in Fig. 2 is a plot of the fitted energy dependence,

$$S\lambda_{in}/G(\rho) = F(E) = E^{d_2}\ln(d_3E), \tag{17}$$

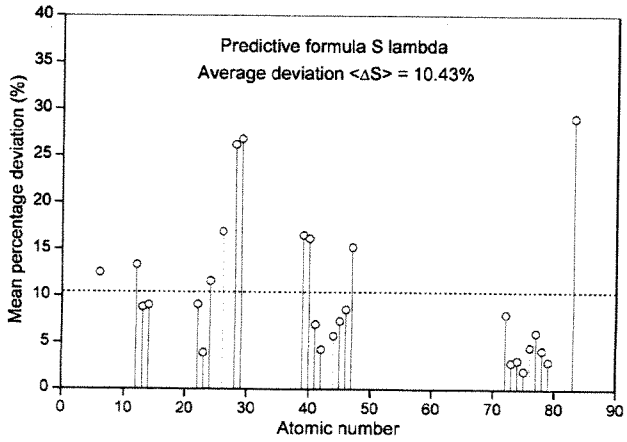

FIG. 6. Mean percentage deviations, $\langle \Delta S_i \rangle$, calculated from Eqs. (3) and (19) as a function of atomic number for the original set of 27 elemental solids (Ref. 18). The dashed line indicates the average value for this group of elements (10.44%).

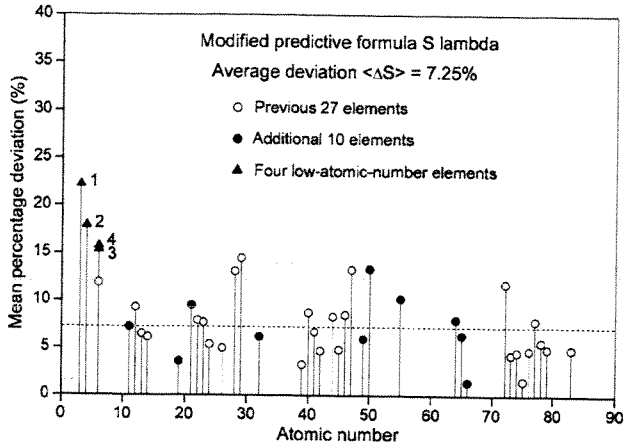

FIG. 7. Mean percentage deviations, $\langle \Delta S_i \rangle$, calculated from Eqs. (16) and (20) as a function of atomic number for our group of 37 elemental solids. Open circles: previously considered group of 27 elements (see Fig. 5); solid circles: additional ten elements. The dashed line indicates the average value for this group of elements (7.25%). The four low-Z elements are indicated by solid triangles: (1) Li, (2) Be, (3) graphite, and (4) diamond.

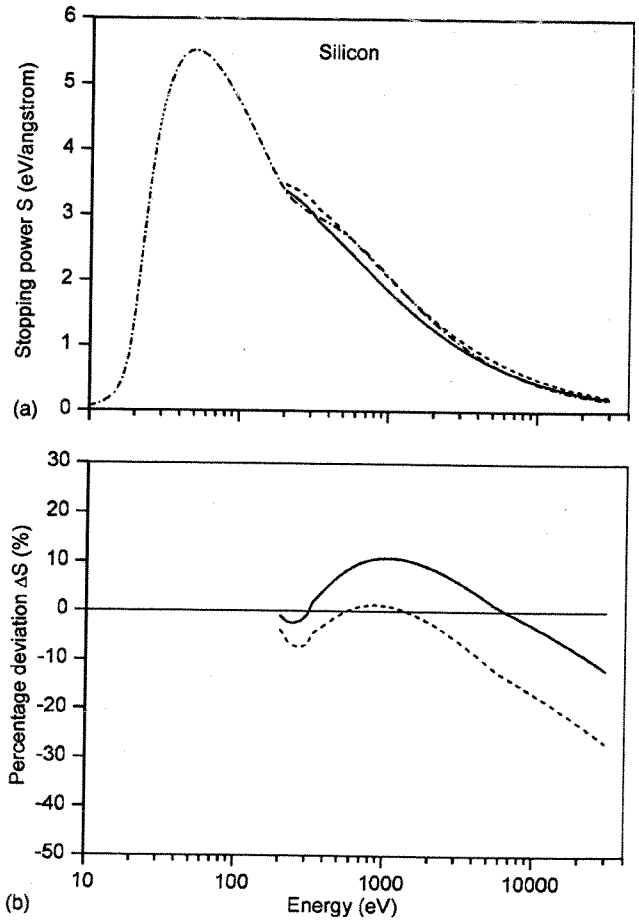

FIG. 8. Comparisons of SPs calculated from optical data for silicon (dot-dashed line) with SPs obtained from the SP predictive formulas. In the upper panel, the dashed line denotes SPs obtained from Eq. (3) and the solid line denotes SPs obtained from the presently proposed predictive formula [Eq. (16)]. The lower panel shows the percentage deviation expressed by Eq. (21) where the dashed line refers to SPs from Eq. (3) and the solid line refers to SPs from Eq. (16).

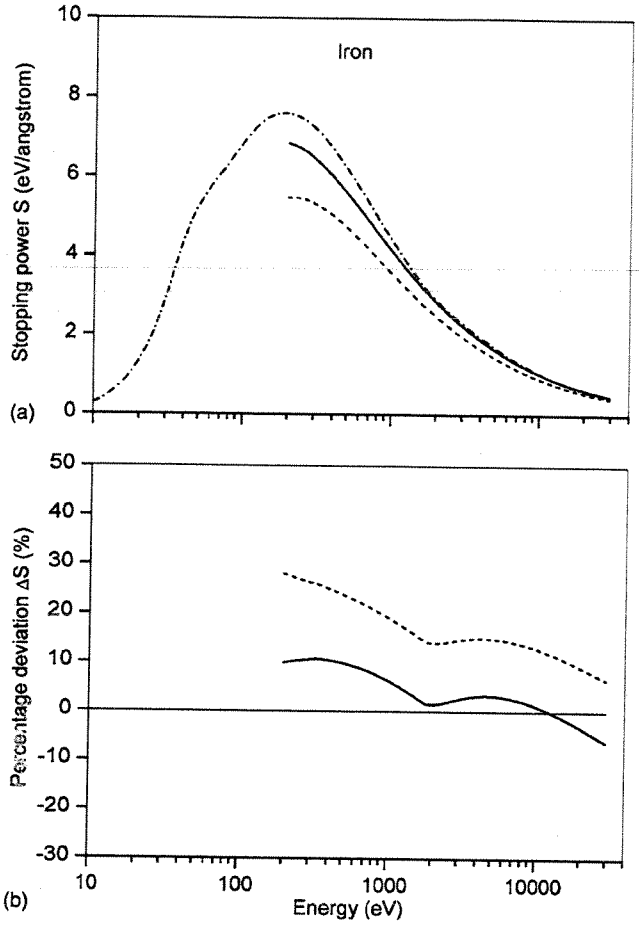

FIG. 9. Same as Fig. 7 except for iron.

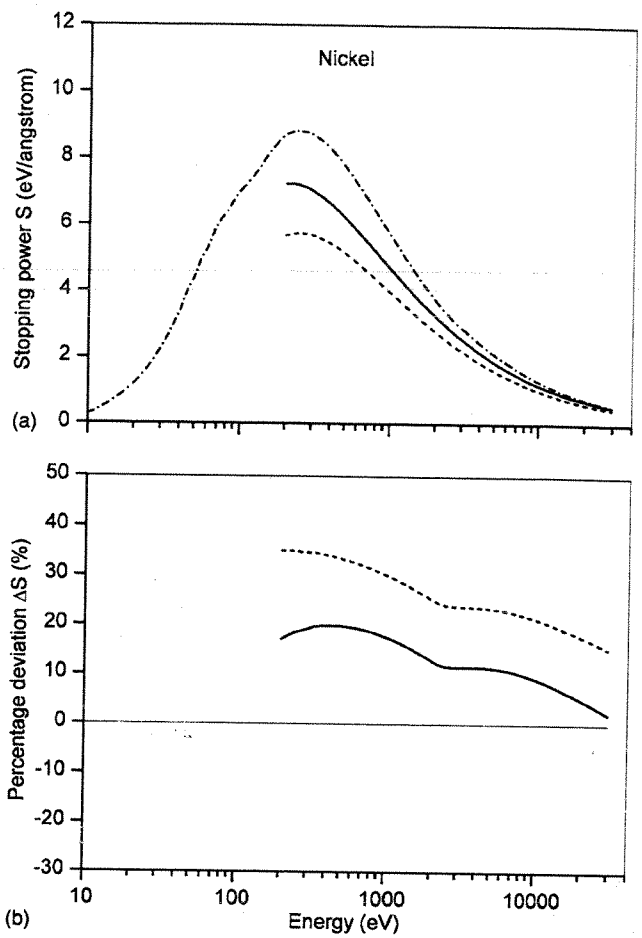

FIG. 10. Same as Fig. 7 except for nickel.

with parameter values from our fit. Equation (17) follows from Eqs. (14) and (16). In Fig. 3, we show the function $S\lambda_{in}/G(\rho)$ calculated for the four low-Z solids, and compare these plots with the shape of the fitted energy dependence. The shapes of these dependences deviate distinctly from the fitted curve for the 37 other solids, despite the fact that SPs for each of the four solids can be well described by Eq. (11) (see Table I).

We plot the function $S\lambda_{in}/F(E)$ for the 37 elemental solids in Fig. 4 to show the dependence on density. We see that this dependence is now very well defined, as indicated by the solid line that shows a plot of Eq. (14) with parameter values determined from the fit. This result confirms that Eq. (14) proposed for describing the density dependence is satisfactory (although there is no known theoretical justification for this expression).

Finally, we attempted to introduce the function $H(Z)$ to make further improvements in the quality of the fit. An obvious choice would be the same function that was used in our earlier study:[18]

$$H(Z) = d_6 Z + 1. \tag{18}$$

We plot the function $S\lambda_{in}/[F(E)G(\rho)]$ in Fig. 5 to visualize the residual dependences on atomic number. We see, however, that the plotted points scatter around unity. Consequently, it is reasonable to assume that $d_6=0$. This conclusion was further confirmed by additional fits. Inclusion of the function $H(Z)$ in the minimization procedure did not decrease further the mean percentage deviation. We therefore conclude that Eq. (16) is suitable for approximating the calculated SPs.

Let us now consider the mean percentage deviation between SPs calculated from Eq. (3) and SPs calculated from optical data, averaged for the ith element over the considered energy range:

$$\langle \Delta S_i \rangle = 100 \frac{1}{N_E} \sum_{j=1}^{N_E} \frac{|S_{i,j} - S_{\text{fit}}(E_j, Z_i)|}{S_{i,j}}. \tag{19}$$

The mean percentage deviations for the previous S-lambda expression [Eq. (3)] are shown as a function of atomic number for the original set of 27 elements in Fig. 6. We note large deviations for Ni, Cu, and Bi. We now calculate similar mean percentage deviations for the presently proposed S-lambda expression [Eq. (16)]:

$$\langle \Delta S_i \rangle = 100 \frac{1}{N_E} \sum_{j=1}^{N_E} \frac{|S_{i,j} - S_{\text{fit}}(E_j, \rho_i)|}{S_{i,j}}. \tag{20}$$

Values of $\langle \Delta S_i \rangle$ from Eq. (20) are shown in Fig. 7 for our group of 37 elements. We see that the improved S-lambda function gives generally smaller deviations than those shown in Fig. 6 for Eq. (3). The proposed predictive formula [Eq.

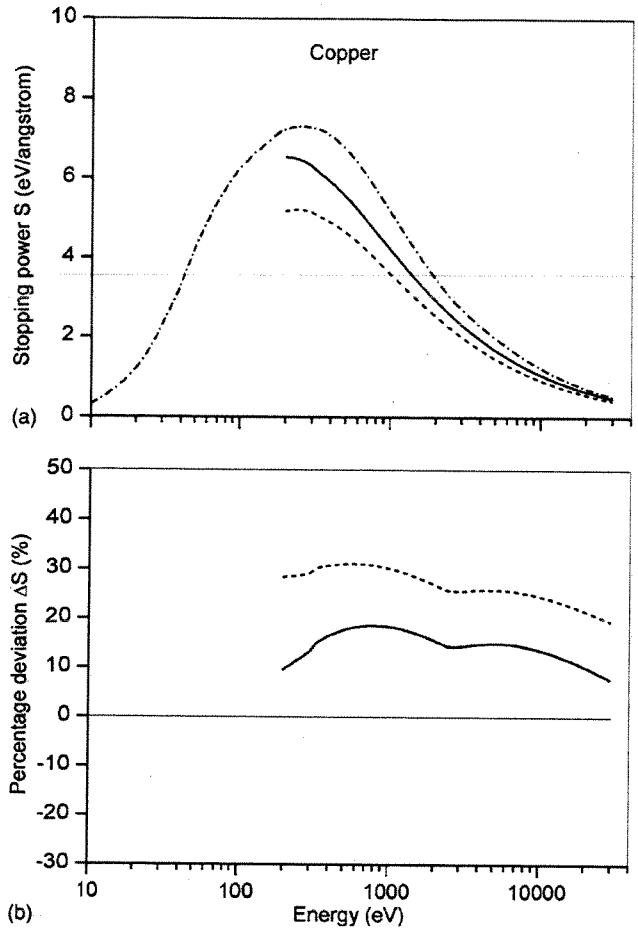

FIG. 11. Same as Fig. 7 except for copper.

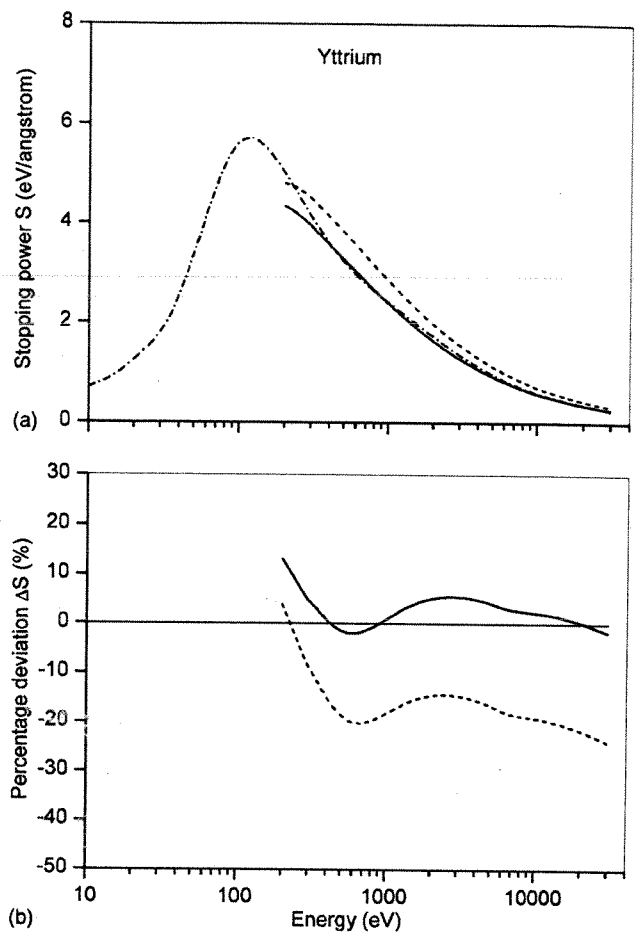

FIG. 12. Same as Fig. 7 except for yttrium.

(16)] with fitted coefficients leads to the following mean percentage deviations for the low-Z materials: 22.18% for Li, 17.92% for Be, 15.34% for graphite, and 15.73% for diamond. These deviations are distinctly larger than the mean percentage deviations for the other elements. As follows from Fig. 7, the values of $\langle \Delta S_i \rangle$ for glassy carbon, Ni, Cu, Ag, and Hf are appreciably larger than for other elements; they are equal to 11.86%, 13.11%, 14.51%, 13.28%, and 11.80%, respectively. On the other hand, the largest values of $\langle \Delta S_i \rangle$ shown in Fig. 6 are observed for Ni, Cu, and Bi (equal to 26.17%, 26.78%, and 29.06%, respectively). The use of the improved predictive formula decreases considerably the mean percentage deviations for these three solids.

It is of interest to compare the calculated and predicted energy dependences of SPs for selected elements in the presently analyzed energy range. These comparisons are shown in the upper panels of Figs. 8–13 for Si, Fe, Ni, Cu, Y, and Bi (which show a reduction in $\langle \Delta S_i \rangle$ from the improved formula) and the upper panel of Fig. 14 for Hf (which shows an increase in $\langle \Delta S_i \rangle$ from the improved formula). In the lower panels, we show the percentage difference,

$$\Delta S = 100 \frac{|S_{\text{calc}} - S_{\text{pred}}|}{S_{\text{calc}}}, \tag{21}$$

where S_{calc} denotes a SP calculated from optical data (for a particular element and energy) and S_{pred} denotes the corresponding SP from one of the predictive formulas, Eq. (3) or Eq. (16). As mentioned above, the best improvement is observed for Ni, Cu, and Bi (Figs. 10, 11, and 13). For Ni and Cu, however, the performance of the improved formula is still not ideal. The maximum deviation reaches 20% for $E < 1$ keV. Equation (3), however, leads to deviations exceeding 30% for this energy range. The improvement for Bi is the most pronounced. SPs from the improved formula deviate from the calculated SPs by less than 10% over the total energy range considered, while deviations of up to 40% are observed with the previous formula. Nevertheless, use of Eq. (16) leads to larger mean percentage deviations for some elements than Eq. (3), as can be seen from Figs. 6 and 7. The largest increase is observed for Hf. Figure 14 shows comparison of Hf SPs from the two predictive formulas with the SPs calculated from optical data. In this case, the maximum percentage difference is 19.11% at 30 keV with the improved formula while previously the deviation at 30 keV was 8.35%. The maximum deviation for Hf with the previous formula was −19.43% (near 300 eV). Although the improved formula performs better for Hf at low energies, the mean percentage deviation is distinctly larger with this formula.

IV. DISCUSSION

Our improved predictive SP formula [Eq. (16)] provides satisfactory fits to a set of calculated SPs and IMFPs for 37

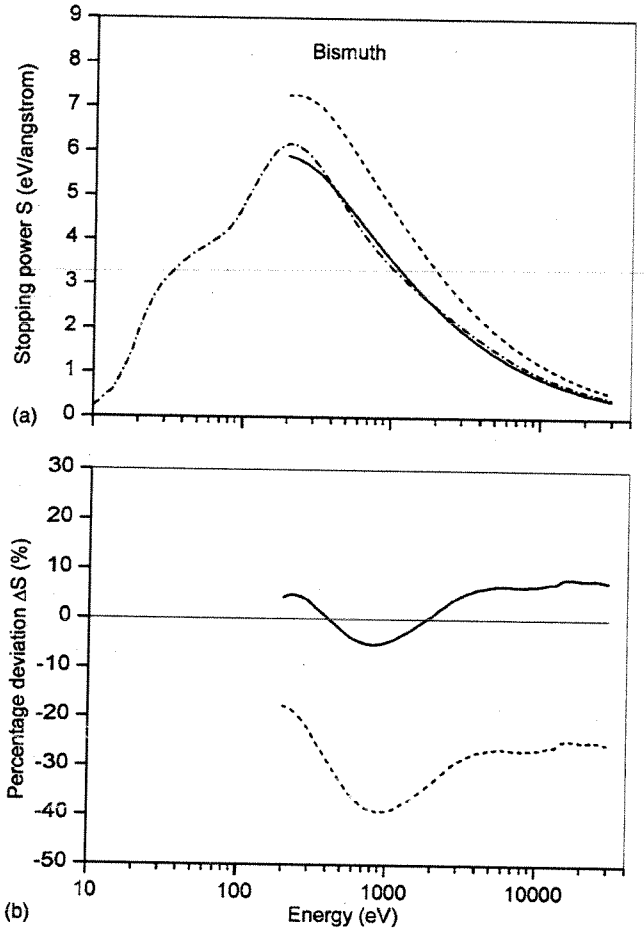

FIG. 13. Same as Fig. 7 except for bismuth.

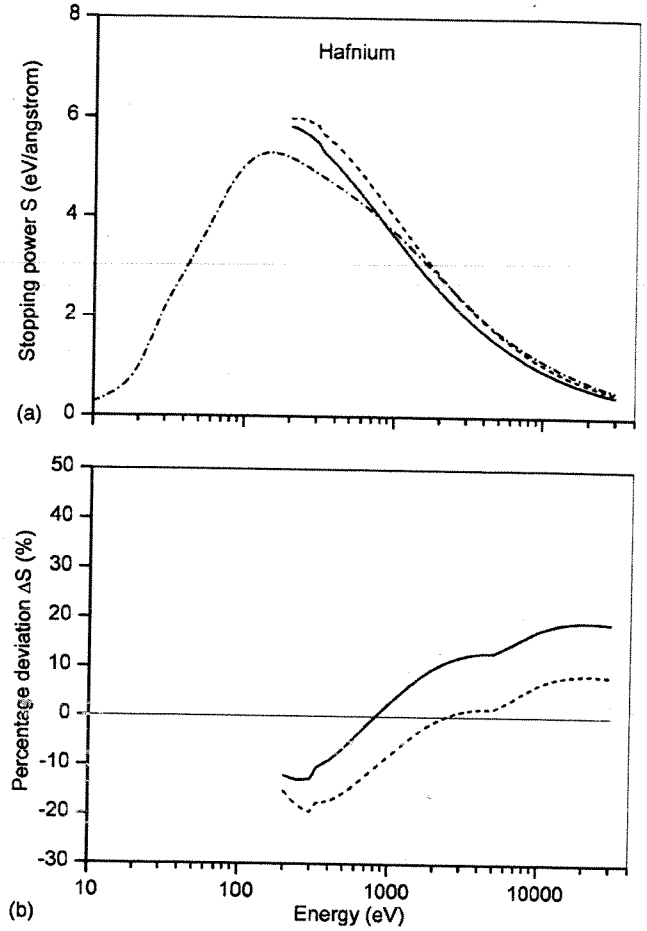

FIG. 14. Same as Fig. 7 except for hafnium.

elemental solids for electron energies between 200 eV and 30 keV. The mean percentage deviation between SPs from Eq. (16) and SPs calculated from optical data was 7.25%, much less than the mean deviation of 10.44% found with our previous SP formula [Eq. (3)] for 27 of these solids. Nevertheless, Eq. (16) does not provide satisfactory fits for four low-Z solids (Li, Be, graphite, and diamond). As previously mentioned, the average percentage deviation between SPs from Eq. (16) and SPs from optical data for these four solids varied between 15.15% and 24.85%. Although the energy dependence of the SPs for the low-Z elements is well described by the expression proposed here [Eq. (11)] (see. Table I), the shapes of these dependences deviate noticeably from the shape of the energy dependence found from fits to the SPs for the other 37 elements, as shown in Fig. 3. Consequently, our predictive formula may, unfortunately, lead to considerable deviations when applied to low-Z elements. This situation is illustrated in Figs. 15 and 16. For Li (Fig. 15), the maximum deviation of SPs from Eq. (3) is 151.73% while the maximum deviation from Eq. (16) is 58.92%, both at 30 keV. For Be (Fig. 16), the maximum deviations are also observed at 30 keV, and are equal to 57.63% and 48.72% for Eqs. (3) and (16), respectively.

Our analysis indicates that the improved predictive SP formula [Eq. (16)] is satisfactory for describing the calculated SPs for our group of 37 elemental solids with $Z>6$. For Li, Be, graphite, and diamond, it is advisable to use Eqs. (11) and (12) with parameter values given in Table I to obtain fitted or interpolated SPs for these solids. The predicted SPs from Eq. (16) for glassy carbon, however, are reasonable, as shown in Figs. 6 and 7. The average deviation between SPs from Eq. (3) and the calculated SPs is 12.51%, while the corresponding deviation from Eq. (16) is 11.86%.

We emphasize that Eq. (16) is an empirical formula and that we do not have a physical basis for the direct dependence on electron energy and sample density. We point out, however, that IMFP values can be estimated from energy, density, atomic or molecular weight, and the bandgap energy for nonconductors [Eq. (24) below]. The dependence of $S_{\text{fit}}(E,\rho)$ on energy and density can therefore be more complex than indicated by Eq. (16).

SP data are frequently needed for MC modeling of electron trajectories. Such calculations provide useful parameters for quantification of AES and EPMA. For example, simulations of primary-electron trajectories over a wide range of energies are made to calculate parameters describing electron backscattering from solids [e.g., the backscattering factor in AES (Refs. 1, 13–15, and 27) and the excitation depth distribution function giving the in-depth distribution of inner-shell ionizations in AES and EPMA].[27] MC simulations can be similarly used in calculations of the radial distribution of Auger-electron emission; this approach facilitates determina-

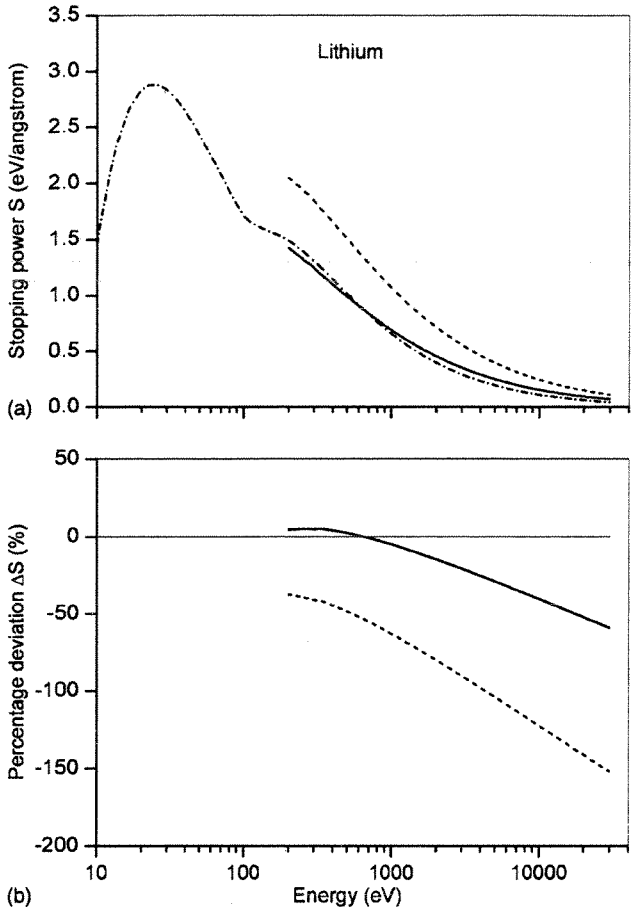

FIG. 15. Comparisons of SPs calculated from optical data for lithium (dot-dashed line) with SPs obtained from the predictive formulas. In the upper panel, the dashed line denotes SPs obtained from Eq. (3) and the solid line denotes SPs obtained from the presently proposed predictive formula [Eq. (16)]. The lower panel shows the percentage deviation expressed by Eq. (21) where the dashed line refers to SPs from Eq. (3) and the solid line refers to SPs from Eq. (16). Note that the lithium data were not considered in the derivation of Eqs. (3) and (16).

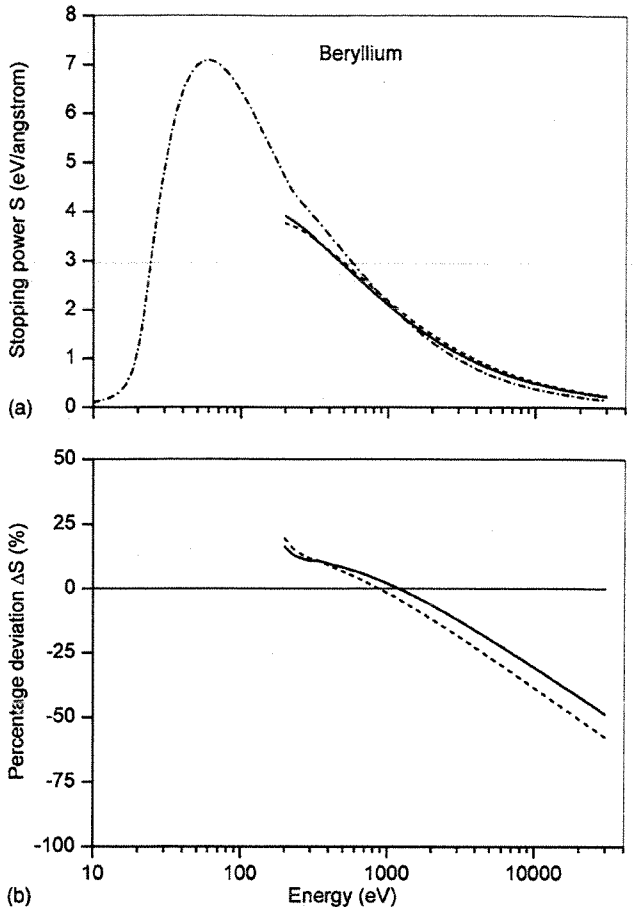

FIG. 16. Same as Fig. 13 except for beryllium.

tion of the lateral resolution of scanning Auger-electron microscopy for the limiting case of an ideal chemical edge.[28]

In practical applications of AES and EPMA, however, alloys and compounds are often analyzed, and MC simulations for quantification need SPs for such materials. Let us consider a multicomponent material consisting of n elements. Following the procedure used for extension of the Bethe SP formula to compounds, the following generalization of the S-lambda expression was proposed previously:[19]

$$S = \sum_{k=1}^{n} C_k \frac{c_1(c_2 Z_k + 1)\ln(c_3 E)}{\lambda_{\text{in}}}$$

$$= \frac{1}{\lambda_{\text{in}}} c_1 \ln(c_3 E)\left(1 + c_2 \sum_{k=1}^{n} C_k Z_k\right) \quad (\text{in eV/Å}), \qquad (22)$$

where C_k is the mass fraction for the kth element. In the case of the SP predictive formula derived here, generalization to alloys or compounds seems straightforward. We propose now to use Eq. (16) in calculations of SPs for compounds, S_{comp}, with values of d_1–d_5 found in the fit to the calculated SPs for the group of 37 elemental solids and to introduce the IMFP and density, ρ_c, of the compound,

$$S_{\text{comp}}(E, \rho_c) = \frac{d_1 E^{d_2} \ln(d_3 E)(\rho_c + d_4)^{d_5}}{\lambda_{\text{in}}}. \qquad (23)$$

Preliminary calculations of S_{comp} have been made for one organic compound (guanine) and one inorganic compound (InSb). Figures 17 and 18 show SPs calculated from optical data for these compounds[23] together with SPs obtained from the previous predictive formula for compounds [Eq. (22)] and the improved predictive formula [Eq. (23)]. We see in Fig. 17 that the deviations of predicted SPs from Eq. (22) for guanine reach 38.3% for $E=200$ eV; nevertheless, SPs from the improved formula are more accurate than the old formula [Eq. (22)] for $E>3$ keV. The percentage deviation reaches 19.5% at 30 keV, as compared with 38.5% for Eq. (22). For InSb in Fig. 18, SPs from the improved predictive formula, over the entire energy range, deviate from the calculated SPs more (with a maximum deviation of 24.9% at 245 eV) than for the previous formula (with a maximum deviation of 14.0% at 221 eV). The mean percentage deviations $\langle \Delta S_i \rangle$ calculated for these two compounds using Eq. (20) [and replacing $S_{\text{fit}}(E, \rho)$ with $S_{\text{comp}}(E, \rho_c)$ given by Eq. (23)] are larger than found for most elemental solids (Fig. 6): 16.0% for guanine and 19.1% for InSb.

IMFPs have been calculated from optical data for only a

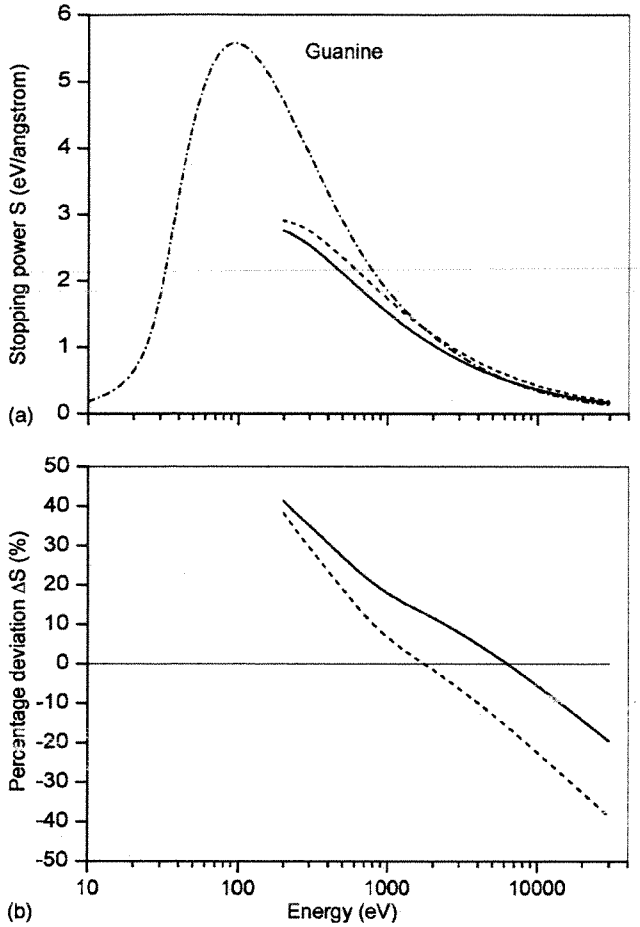

FIG. 17. (a) Comparisons of SPs calculated from optical data for guanine (dot-dashed line) with SPs obtained from the two predictive formulas. The dashed line denotes SPs obtained from the previously proposed formula for compounds [Eq. (22)] and the solid line denotes SPs obtained from the presently proposed formula [Eq. (23)]. (b) Percentage deviations expressed by Eq. (21) between SPs from the two predictive formulas, Eq. (22) (dashed line) and Eq. (23) (solid line), and SPs calculated from optical data.

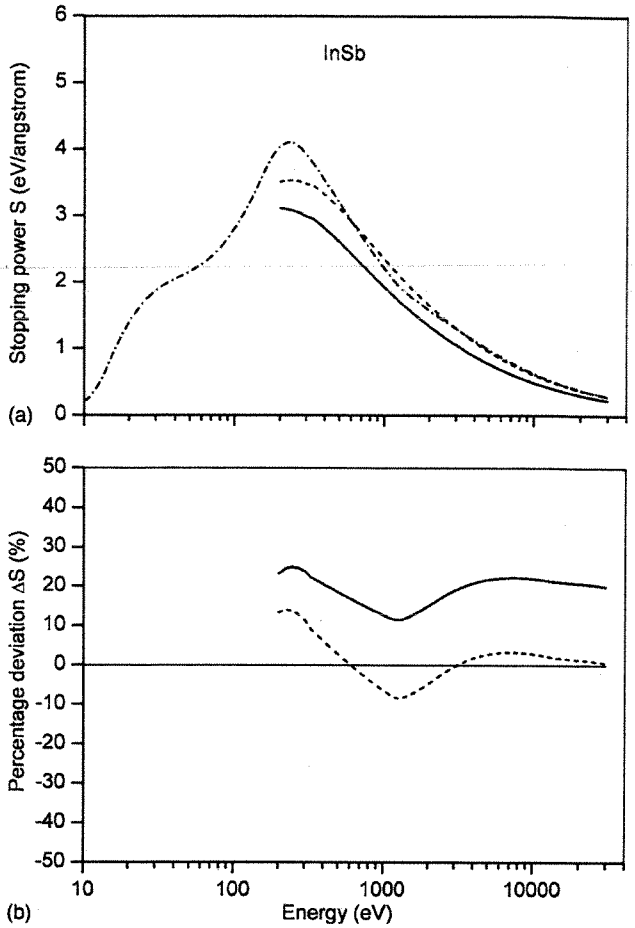

FIG. 18. Same as Fig. 15 except for indium antimonide.

very limited number of compounds. It is then necessary to compute IMFPs for most compounds [for use in Eq. (23)] from the TPP-2M predictive formula:[29]

$$\lambda_{\text{in}} = \frac{E}{E_p^2[\beta \ln(\gamma E) - (C/E) + (D/E^2)]} \quad (\text{in Å}),$$

$$\beta = -0.10 + 0.944(E_p^2 + E_g^2)^{-1/2} + 0.069\rho^{0.1},$$

$$\gamma = 0.191\rho^{-1/2},$$

$$C = 1.97 - 0.91U, \tag{24}$$

$$D = 53.4 - 20.8U,$$

$$U = N_v\rho/A = E_p^2/829.4,$$

where $E_p = 28.8(N_v\rho/A)^{1/2}$ is the free-electron plasmon energy (in eV), N_v is the number of valence electrons per atom (for elemental solids) or molecule (for compounds), A denotes here the atomic or molecular weight, and E_g is the bandgap energy (in eV). We see that the SP for a given element or multicomponent solid, expressed by Eqs. (16) and (24) for elemental solids or Eqs. (23) and (24) for alloys and compounds, can be determined from four material parameters: density, molecular weight, bandgap energy, and number of valence electrons per molecule. The accuracy of this procedure for multicomponent solids may be rather limited at present, as follows from Figs. 17 and 18. We plan to make more extensive comparisons of calculated SPs and IMFPs from Eqs. (23) and (24) with SPs calculated from optical data for other compounds for which the needed optical data are available.

V. SUMMARY

We have developed an improved predictive formula [Eq. (16)] for the electron SP based on a combined fit to SPs and IMFPs calculated from optical data for 37 elemental solids and energies between 200 eV and 30 keV. The improved formula, a function of electron energy, density, and IMFP, yielded a mean deviation between predicted SPs and calculated SPs of 7.25%, a value lower than that found from our earlier predictive SP formula (10.44%).[18]

Large average deviations were found for four other materials, Li (22.2%), Be (17.9%), graphite (15.3%), and diamond (15.7%), in comparisons of SPs from Eq. (16) and the calculated SPs. Although the energy dependence of the SPs for these four low-Z materials is well described by a similar

expression [Eq. (11)], the shapes of these dependences deviate noticeably from the shape of the energy dependence found from fits to SPs for the other 37 solids [Eq. (16)]. We were unable to find any simple dependence on atomic number that would provide a better fit for the complete group of 41 elemental solids. We therefore recommend use of Eq. (16) only for $Z>6$. For Li, Be, graphite, and diamond, we recommend use of Eqs. (11) and (12) with the corresponding parameter values in Table I.

We have generalized our predictive SP equation to apply to multicomponent materials (i.e., compounds and alloys). Equation (23) can be used for this purpose with the same parameter values as for Eq. (16) but now with the density and IMFP of the compound or alloy. We tested Eq. (23) with SPs calculated from optical data for guanine and indium antimonide. While relatively large average deviations of 16.0% and 19.1%, respectively, were found between predicted and calculated SPs for these two compounds, we plan to investigate the validity for a range of organic and inorganic compounds.

ACKNOWLEDGMENTS

One of the authors (A.J.) wishes to acknowledge partial support by Grants No. N204 0769 33.

[1]A. Jablonski, C. J. Powell, and S. Tanuma, Surf. Interface Anal. 37, 861 (2005).
[2]H. A. Bethe, Ann. Phys. 5, 325 (1930); *Handbook of Physics* (Springer, Berlin, 1933), Vol. 24; H. A. Bethe and J. Ashkin, *Experimental Nuclear Physics* (Wiley, New York, 1953).
[3]"Stopping powers for electrons and positrons," International Commission on Radiation Units and Measurements Report No. 37, 1984.
[4]M. J. Berger, J. S. Coursey, and M. A. Zucker, Stopping-Power and Range Tables for Electrons, Positrons and Helium Ions, NIST Physical Reference Data, web address: http://physics.nist.gov/PhysRefData/Star/Text/contents.html.
[5]D. C. Joy, A Database of Electron-Solid Interactions, web address: http://pciserver.bio.utk.edu/metrology.
[6]M. Inokuti, Rev. Mod. Phys. 43, 297 (1971).
[7]J. Goldstein, D. Improvedbury, D. Joy, C. Lyman, P. Echlin, E. Lifshin, L. Sawyer, and J. Michael, *Scanning Electron Microscopy and X-Ray Microanalysis* (Springer, New York, 2003), p. 63.
[8]S. Tanuma, C. J. Powell, and D. R. Penn, Surf. Interface Anal. 37, 978 (2005).
[9]T. S. Rao-Sahib and D. B. Wittry, J. Appl. Phys. 45, 5060 (1974).
[10]G. Love, M. G. C. Cox, and V. D. Scott, J. Phys. D 10, 7 (1977).
[11]D. C. Joy and S. Luo, Scanning 11, 176 (1989).
[12]J. M. Fernandez-Varea, R. Mayol, D. Liljequist, and F. Salvat, J. Phys.: Condens. Matter 5, 3593 (1993).
[13]R. Shimizu and S. Ichimura, "Quantitative analysis by Auger electron spectroscopy," Toyota Foundation Research Report No. I-006 76-0175, 1981.
[14]S. Ichimura and R. Shimizu, Surf. Sci. 112, 386 (1981).
[15]R. Shimizu, Jpn. J. Appl. Phys., Part 1 22, 1631 (1983).
[16]S. Ichimura, M. Aratama, and R. Shimizu, J. Appl. Phys. 51, 2853 (1980).
[17]S. Tougaard, Solid State Commun. 61, 547 (1987); Surf. Interface Anal. 25, 137 (1997).
[18]A. Jablonski, S. Tanuma, and C. J. Powell, Surf. Interface Anal. 38, 76 (2006).
[19]A. Jablonski, S. Tanuma, and C. J. Powell, J. Surf. Anal. 13, 170 (2006).
[20]C. J. Powell and A. Jablonski, J. Phys. Chem. Ref. Data 28, 19 (1999).
[21]D. R. Penn, Phys. Rev. B 35, 482 (1987).
[22]S. Tanuma, C. J. Powell, and D. R. Penn (unpublished).
[23]S. Tanuma, C. J. Powell, and D. R. Penn, J. Appl. Phys. 103, 063707 (2008).
[24]S. Tanuma, C. J. Powell, and D. R. Penn, Surf. Interface Anal. 11, 577 (1988).
[25]S. Tanuma, C. J. Powell, and D. R. Penn, J. Electron Spectrosc. Relat. Phenom. 62, 95 (1993).
[26]S. Tanuma, C. J. Powell, and D. R. Penn, Surf. Interface Anal. 37, 1 (2005).
[27]A. Jablonski and C. J. Powell, Surf. Sci. 574, 219 (2005); 601, 965 (2007).
[28]A. Jablonski and C. J. Powell, Appl. Surf. Sci. 242, 220 (2005).
[29]S. Tanuma, C. J. Powell, and D. R. Penn, Surf. Interface Anal. 21, 165 (1994).